

**DIFFRACTION BY A TERMINATED, SEMI-INFINITE
PARALLEL-PLATE WAVEGUIDE WITH FOUR-LAYER
MATERIAL LOADING: THE CASE OF H
POLARIZATION**

E. H. Shang and K. Kobayashi

Department of Electrical, Electronic, and Communication
Engineering
Chuo University
Tokyo 112-8551, Japan

Abstract—The diffraction by a terminated, semi-infinite parallel-plate waveguide with four-layer material loading is rigorously analyzed for the H -polarized plane wave incidence by means of the Wiener-Hopf technique. Introducing the Fourier transform for the unknown scattered field and applying boundary conditions in the transform domain, the problem is formulated in terms of the simultaneous Wiener-Hopf equations. The Wiener-Hopf equations are solved via the factorization and decomposition procedure together with the use of the edge condition leading to exact and approximate solutions. The scattered field inside and outside the waveguide is evaluated by taking the inverse Fourier transform and applying the saddle point method. Numerical examples on the radar cross section (RCS) are presented for various physical parameters, and the backscattering characteristics of the waveguide are discussed.

1. INTRODUCTION

The analysis of the scattering by open-ended waveguide cavities is an important subject in the prediction and reduction of the radar cross section (RCS) of a target [1–4]. There are a number of papers treating two-dimensional (2-D) and three-dimensional (3-D) cavity diffraction problems based on high-frequency ray techniques and numerical methods [5–11], but the solutions obtained by these approaches may not be uniformly valid for arbitrary cavity dimensions.

Corresponding author: K. Kobayashi (kazuya@kazuya.elect.chuo-u.ac.jp).

The Wiener-Hopf technique [12–14] is known as a powerful tool for analyzing wave scattering and diffraction problems related to canonical structures rigorously. There are some important contributions to studies on the cavity RCS by Büyükkaksoy et al. [15, 16] based on the Wiener-Hopf technique. In the previous papers [17–24], we have also considered several 2-D cavities formed by a finite parallel-plate waveguide, and analyzed the problem of the plane wave diffraction rigorously using the Wiener-Hopf technique. It has been clarified that our final results presented in [17–24] are valid for the cavity depth greater than the incident wavelength. As a related 2-D cavity geometry, we have subsequently considered a semi-infinite parallel-plate waveguide with an interior planar termination, and carried out the Wiener-Hopf analysis of the plane wave diffraction [25, 26]. It is important to note that the cavity in [25, 26] is formed by a semi-infinite parallel-plate waveguide and hence, our solutions are uniformly valid for arbitrary cavity dimensions.

In [25, 26], we have treated the case where the planar termination inside the waveguide is loaded with a three-layer material. As an important generalization of our previous analysis [25, 26], we have considered in [27] a terminated, semi-infinite parallel-plate waveguide with four-layer material loading, and analyzed the E -polarized plane wave diffraction rigorously by using the Wiener-Hopf technique. It should be noted that the solution obtained in [27] is uniformly valid for arbitrary cavity dimensions. We have also verified by numerical computation that the four-layer material loading inside the cavity leads to better RCS reduction in comparison to the three-layer case. In this paper, we shall consider the same waveguide geometry as in [27], and analyze the diffraction problem for the H -polarized plane wave incidence by means of the Wiener-Hopf technique.

Introducing the Fourier transform for the unknown scattered field and applying boundary conditions in the transform domain, the problem is formulated in terms of the simultaneous Wiener-Hopf equations. The Wiener-Hopf equations are then solved via the factorization and decomposition procedure leading to the exact solution. It should be noted, however, that this solution is formal since an infinite number of unknowns are contained. By using the edge condition, an approximate solution efficient for numerical computation is explicitly derived, which involves numerical inversion of finite-size matrix equations. Taking the inverse Fourier transform and using the saddle point method, a scattered field expression inside and outside the waveguide is evaluated analytically. Representative numerical examples on the RCS are presented, and the far field backscattering characteristics of the waveguide are discussed in detail.

Some comparisons with the E -polarized case [27] will also be given. Since the method of solution employed here is similar to that in [27], only the main results will be summarized.

The time factor is assumed to be $e^{-i\omega t}$, and suppressed throughout this paper.

2. FORMULATION OF THE PROBLEM

The geometry of the problem is shown in Fig. 1, where the waveguide plates are infinitely thin, perfectly conducting, and uniform in the y -direction. The material layers I ($-d_1 < z < -d_2$), II ($-d_2 < z < -d_3$), III ($-d_3 < z < -d_4$), and IV ($-d_4 < z < -d_5$) are characterized by the relative permittivity/permeability (ε_m, μ_m) for $m = 1, 2, 3$, and 4, respectively.

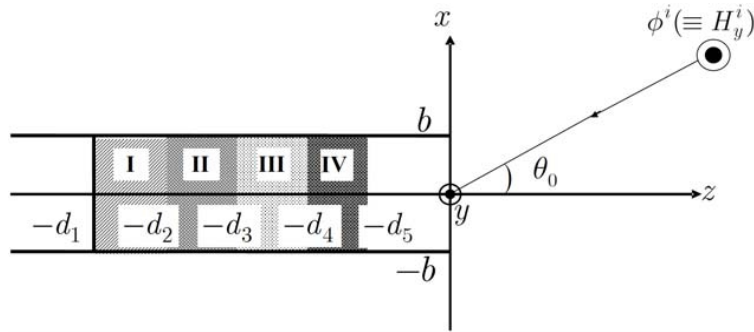


Figure 1. Geometry of the problem.

Let the total magnetic field $\phi^t(x, z) [\equiv H_y^t(x, z)]$ be

$$\phi^t(x, z) = \phi^i(x, z) + \phi(x, z), \quad (1)$$

where $\phi^i(x, z)$ is the incident field of H polarization defined by

$$\phi^i(x, z) = e^{-ik(x \sin \theta_0 + z \cos \theta_0)}, \quad 0 < \theta_0 < \pi/2, \quad (2)$$

where $k [\equiv \omega(\mu_0\varepsilon_0)^{1/2}]$ is the free-space wavenumber. We shall assume that the vacuum is slightly lossy as in $k = k_1 + ik_2$ with $0 < k_2 \ll k_1$. The total field $\phi^t(x, z)$ satisfies the 2-D Helmholtz equation

$$[\partial^2/\partial x^2 + \partial^2/\partial z^2 + \mu(x, z)\varepsilon(x, z)k^2] \phi^t(x, z) = 0, \quad (3)$$

where

$$\mu(x, z) = \begin{cases} \mu_1(\text{layer I}) \\ \mu_2(\text{layer II}) \\ \mu_3(\text{layer III}) \\ \mu_4(\text{layer IV}) \\ 1(\text{otherwise}) \end{cases}, \quad \varepsilon(x, z) = \begin{cases} \varepsilon_1(\text{layer I}) \\ \varepsilon_2(\text{layer II}) \\ \varepsilon_3(\text{layer III}) \\ \varepsilon_4(\text{layer IV}) \\ 1(\text{otherwise}) \end{cases}. \quad (4)$$

Once the solution of (3) has been found, nonzero components of the total electromagnetic fields are derived from

$$(H_y^t, E_x^t, E_z^t) = \left[\phi^t, \frac{1}{i\omega\varepsilon_0\varepsilon(x, z)} \frac{\partial \phi^t}{\partial z}, \frac{i}{\omega\varepsilon_0\varepsilon(x, z)} \frac{\partial \phi^t}{\partial x} \right]. \quad (5)$$

It follows from the radiation condition that

$$\begin{aligned} \phi(x, z) &= O\left(e^{k_2 z \cos \theta_0}\right) \quad \text{as } z \rightarrow -\infty, \\ &= O\left(e^{-k_2 z}\right) \quad \text{as } z \rightarrow \infty. \end{aligned} \quad (6)$$

Let us define the Fourier transform of the scattered field as

$$\begin{aligned} \Phi(x, \alpha) &= (2\pi)^{-1/2} \int_{-\infty}^{\infty} \phi(x, z) e^{i\alpha z} dz, \\ \alpha &= \text{Re } \alpha + i\text{Im } \alpha (\equiv \sigma + i\tau). \end{aligned} \quad (7)$$

Introducing the Fourier integrals as

$$\Phi_+(x, \alpha) = (2\pi)^{-1/2} \int_0^{\infty} \phi(x, z) e^{i\alpha z} dz, \quad (8)$$

$$\Phi_-(x, \alpha) = (2\pi)^{-1/2} \int_{-\infty}^{d_1} \phi(x, z) e^{i\alpha z} dz, \quad (9)$$

$$\begin{aligned} \Phi_1^{(m)}(x, \alpha) &= (2\pi)^{-1/2} \int_{-d_m}^{-d_{m+1}} \phi^t(x, z) e^{i\alpha z} dz \\ &\quad \text{for } m = 1, 2, 3, 4, \end{aligned} \quad (10)$$

$$\Phi_1^{(5)}(x, \alpha) = (2\pi)^{-1/2} \int_{-d_5}^0 \phi^t(x, z) e^{i\alpha z} dz, \quad (11)$$

we can express $\Phi(x, \alpha)$ as

$$\begin{aligned} \Phi(x, \alpha) &= \Psi_{(+)}(x, \alpha) + \Phi_-(x, \alpha) \quad \text{for } |x| > b, \\ &= \Psi_{(+)}(x, \alpha) + \Phi_1(x, \alpha) \quad \text{for } |x| < b \end{aligned} \quad (12)$$

by using (8)–(11), where

$$\Psi_{(+)}(x, \alpha) = \Phi_{+}(x, \alpha) - \frac{e^{-ikx \sin \theta_0}}{(2\pi)^{1/2}i(\alpha - k \cos \theta_0)}, \quad (13)$$

$$\Phi_1(x, \alpha) = \sum_{m=1}^5 \Phi_1^{(m)}(x, \alpha). \quad (14)$$

In view of the radiation condition, it follows that $\Phi(x, \alpha)$, $\Phi_{+}(x, \alpha)$, and $\Phi_{-}(x, \alpha)$ are regular in $-k_2 < \tau < k_2 \cos \theta_0$, $\tau > -k_2$, and $\tau < k_2 \cos \theta_0$, respectively, whereas $\Phi_1^{(m)}(x, \alpha)$ for $m = 1, 2, 3, 4, 5$ are entire functions. We also note that $\Psi_{(+)}(x, \alpha)$ is regular in $\tau > -k_2$ except for a simple pole at $\alpha = k \cos \theta_0$. We shall henceforth use these conventions for indicating the regions of regularity of functions in the complex α -plane.

Taking the Fourier transform and the Fourier integrations of (3) and solving the resultant equations by following a procedure similar to that developed in [27], we derive a scattered field representation in the Fourier transform domain with the result that

$$\begin{aligned} \Phi(x, \alpha) &= -\Psi'_{(+)}(\pm b, \alpha)\gamma^{-1}e^{\mp\gamma(x\mp b)} \quad \text{for } x \gtrless \pm b, \\ &= \Psi'_{(+)}(b, \alpha)\frac{\cosh \gamma(x+b)}{\gamma \sinh 2\gamma b} \\ &\quad - \Psi'_{(+)}(-b, \alpha)\frac{\cosh \gamma(x-b)}{\gamma \sinh 2\gamma b} \\ &\quad - \frac{1}{b} \sum_{n=0}^{\infty} \nu_n \frac{c_{5n}(\alpha)}{\alpha^2 + \gamma_n^2} \cos \frac{n\pi}{2b}(x+b) \\ &\quad - \frac{1}{b} \sum_{m=1}^4 \sum_{n=0}^{\infty} \nu_n \frac{c_{mn}(\alpha)}{\alpha^2 + \Gamma_{mn}^2} \cos \frac{n\pi}{2b}(x+b) \end{aligned} \quad \text{for } |x| < b, \quad (15)$$

where $\gamma = (\alpha^2 - k^2)^{1/2}$ with $\text{Re } \gamma > 0$, and

$$\begin{aligned} \nu_n &= 1/2 \quad \text{for } n = 0, \\ &= 1 \quad \text{for } n \geq 1, \end{aligned} \quad (16)$$

$$\begin{aligned} \gamma_n &= -ik \quad \text{for } n = 0, \\ &= [(n\pi/2b)^2 - k^2]^{1/2} \quad \text{for } n \geq 1, \end{aligned} \quad (17)$$

$$\begin{aligned} \Gamma_{mn} &= -ik_m \quad \text{for } n = 0, \\ &= [(n\pi/2b)^2 - k_m^2]^{1/2} \quad \text{for } n \geq 1, \end{aligned} \quad (18)$$

$$k_m = (\mu_m \varepsilon_m)^{1/2} k \quad \text{for } m = 1, 2, 3, 4, \quad (19)$$

$$c_{mn}(\alpha) = e^{-i\alpha d_m} c_{mn}^+(\alpha) - e^{-i\alpha d_{m+1}} c_{(m+1)n}^-(\alpha) \quad (20)$$

for $m = 1, 2, 3, 4,$

$$c_{5n}(\alpha) = e^{-i\alpha d_5} c_{5n}^-(\alpha), \quad (21)$$

$$c_{1n}^+(\alpha) = f_n^+, \quad c_{2n}^-(\alpha) = f_{1n} - i\alpha g_{1n}, \quad (22)$$

$$c_{2n}^+(\alpha) = (\varepsilon_2/\varepsilon_1) f_{1n} - i\alpha g_{1n}, \quad c_{3n}^-(\alpha) = f_{2n} - i\alpha g_{2n}, \quad (23)$$

$$c_{3n}^+(\alpha) = (\varepsilon_3/\varepsilon_2) f_{2n} - i\alpha g_{2n}, \quad c_{4n}^-(\alpha) = f_{3n} - i\alpha g_{3n}, \quad (24)$$

$$c_{4n}^+(\alpha) = (\varepsilon_4/\varepsilon_3) f_{3n} - i\alpha g_{3n}, \quad c_{5n}^-(\alpha) = f_{4n} - i\alpha g_{4n}. \quad (25)$$

In (15), the prime denotes differentiation with respect to x . Equation (15) is the scattered field expression in the transform domain. The coefficients f_n^+ , f_{mn} , and g_{mn} in (22)–(25) are defined in Appendix A.

We now differentiate (15) with respect to x and set $x = b \pm 0$, $-b \pm 0$ in the results. Making use of the boundary conditions, we obtain that

$$J_-^d(\alpha) = -\frac{U_{(+)}(\alpha)}{M(\alpha)} - \frac{2}{b} \sum_{n=1, \text{odd}}^{\infty} \left[\frac{c_{5n}(\alpha)}{\alpha^2 + \gamma_n^2} + \sum_{m=1}^4 \frac{c_{mn}(\alpha)}{\alpha^2 + \Gamma_{mn}^2} \right], \quad (26)$$

$$J_-^s(\alpha) = -\frac{V_{(+)}(\alpha)}{N(\alpha)} + \frac{2}{b} \sum_{n=0, \text{even}}^{\infty} \nu_n \left[\frac{c_{5n}(\alpha)}{\alpha^2 + \gamma_n^2} + \sum_{m=1}^4 \frac{c_{mn}(\alpha)}{\alpha^2 + \Gamma_{mn}^2} \right], \quad (27)$$

where

$$U_{(+)}(\alpha) = \Psi'_{(+)}(b, \alpha) + \Psi'_{(+)}(-b, \alpha), \quad (28)$$

$$V_{(+)}(\alpha) = \Psi'_{(+)}(b, \alpha) - \Psi'_{(+)}(-b, \alpha), \quad (29)$$

$$J_-^{d,s}(\alpha) = J_-(b, \alpha) \mp J_-(-b, \alpha), \quad (30)$$

$$J_-(\pm b, \alpha) = \Phi_-(\pm b \pm 0, \alpha) - \Phi_1(\pm b \mp 0, \alpha), \quad (31)$$

$$M(\alpha) = \gamma e^{-\gamma b} \cosh \gamma b, \quad N(\alpha) = \gamma e^{-\gamma b} \sinh \gamma b. \quad (32)$$

Equations (26) and (27) are the desired, simultaneous Wiener-Hopf equations, where $M(\alpha)$ and $N(\alpha)$ are kernel functions.

3. SOLUTION OF THE WIENER-HOPF EQUATIONS

The kernel functions are factorized as [12, 13]

$$M(\alpha) = M_+(\alpha)M_-(\alpha), \quad N(\alpha) = N_+(\alpha)N_-(\alpha), \quad (33)$$

where

$$\begin{aligned}
 M_+(\alpha)[= M_-(-\alpha)] &= (\cos kb)^{1/2} e^{i3\pi/4} \\
 &\cdot (k + \alpha)^{1/2} \exp\{(i\gamma b/\pi) \ln[(\alpha - \gamma)/k]\} \\
 &\cdot \exp\{(i\alpha b/\pi) [1 - C + \ln(\pi/2kb) + i\pi/2]\} \\
 &\cdot \prod_{n=1, \text{odd}}^{\infty} (1 + \alpha/i\gamma_n) e^{2i\alpha b/n\pi}, \quad (34)
 \end{aligned}$$

$$\begin{aligned}
 N_+(\alpha)[= N_-(-\alpha)] &= (k \sin kb)^{1/2} \exp(i\pi/2) \\
 &\cdot \exp\{(i\gamma b/k) \ln[(\alpha - \gamma)/k]\} \\
 &\cdot \exp\{(i\alpha b/\pi) [1 - C + \ln(2\pi/kb) + i\pi/2]\} \\
 &\cdot (1 + \alpha/i\gamma_0) \prod_{n=2, \text{even}}^{\infty} (1 + \alpha/i\gamma_n) e^{2i\alpha b/n\pi} \quad (35)
 \end{aligned}$$

with $C(= 0.57721566 \dots)$ being Euler's constant.

We multiply both sides of (26) and (27) by $M_-(\alpha)$ and $N_-(\alpha)$, respectively, and decompose the results with the aid of the edge condition. After some manipulations, we arrive at

$$U_{(+)}(\alpha) = b^{1/2} M_+(\alpha) \left[-\frac{A}{b(\alpha - k \cos \theta_0)} - \sum_{n=1}^{\infty} \frac{\delta_{2n-1} a_n p_n u_n}{b(\alpha + i\gamma_{2n-1})} \right], \quad (36)$$

$$V_{(+)}(\alpha) = b^{1/2} N_+(\alpha) \left[\frac{B}{b(\alpha - k \cos \theta_0)} - \sum_{n=1}^{\infty} \frac{\nu_{2n-2} \delta_{2n-2} b_n q_n v_n}{b(\alpha + i\gamma_{2n-2})} \right], \quad (37)$$

where δ_n is defined by (A20) in Appendix A, and

$$a_n = (bi\gamma_{2n-1})^{-1}, \quad b_n = (bi\gamma_{2n-2})^{-1}, \quad (38)$$

$$p_n = b^{1/2} M_+(i\gamma_{2n-1}), \quad q_n = b^{1/2} N_+(i\gamma_{2n-2}), \quad (39)$$

$$u_n^+ = U_{(+)}(i\gamma_{2n-1}), \quad v_n^+ = V_{(+)}(i\gamma_{2n-2}), \quad (40)$$

$$A = -\left(\frac{2b}{\pi}\right)^{1/2} \frac{k \sin \theta_0 \cos(kb \sin \theta_0)}{M_+(k \cos \theta_0)}, \quad (41)$$

$$B = -\left(\frac{2b}{\pi}\right)^{1/2} \frac{ik \sin \theta_0 \sin(kb \sin \theta_0)}{N_+(k \cos \theta_0)}. \quad (42)$$

Equations (36) and (37) are the exact solutions to the Wiener-Hopf equations (26) and (27), respectively.

Taking into account the edge condition, we find that

$$u_n^+ \sim -2^{1/2} i K_u(b\gamma_{2n-1})^{-1/2}, \quad v_n^+ \sim -2^{1/2} i K_v(b\gamma_{2n})^{-1/2} \quad (43)$$

as $n \rightarrow \infty$, where K_u and K_v are unknown constants. Approximate expressions of (36) and (37) are derived by using (43) as

$$U_{(+)}(\alpha) \approx b^{1/2} M_+(\alpha) \left[-\frac{A}{b(\alpha - k \cos \theta_0)} - \sum_{n=1}^{N-1} \frac{\delta_{2n-1} a_n p_n u_n^+}{b(\alpha + i\gamma_{2n-1})} - K_u S_u(\alpha) \right], \quad (44)$$

$$V_{(+)}(\alpha) \approx b^{1/2} N_+(\alpha) \left[\frac{B}{b(\alpha - k \cos \theta_0)} - \sum_{n=1}^{N-1} \frac{\nu_{2n-2} \delta_{2n-2} b_n q_n v_n^+}{b(\alpha + i\gamma_{2n-2})} - K_v S_v(\alpha) \right] \quad (45)$$

with N being a large positive integer, where

$$S_u(\alpha) = \sum_{n=N}^{\infty} \frac{\delta_{2n-1} (b\gamma_{2n-1})^{-1}}{b(\alpha + i\gamma_{2n-1})}, \quad (46)$$

$$S_v(\alpha) = \sum_{n=N}^{\infty} \frac{\delta_{2n-2} (b\gamma_{2n-2})^{-1}}{b(\alpha + i\gamma_{2n-2})}. \quad (47)$$

The unknowns u_n^+ and v_n^+ for $n = 1, 2, 3, \dots, N-1$ as well as K_u and K_v are involved in (44) and (45), which can be determined by solving two sets of $N \times N$ matrix equations numerically (see discussion in [27]).

4. SCATTERED FIELD

The scattered field in the real space can be derived by taking the inverse Fourier transform of (15) according to the formula

$$\phi(x, z) = (2\pi)^{-1/2} \int_{-\infty+ic}^{\infty+ic} \Phi(x, \alpha) e^{-i\alpha z} d\alpha, \quad -k_2 < c < k_2 \cos \theta_0. \quad (48)$$

Substituting (15) into (48) and evaluating the resultant integral for $|x| < b$ with the aid of (36) and (37), the scattered field inside the waveguide is derived as

$$\phi(x, z) = -\phi^i(x, z) + \sum_{n=0}^{\infty} T_{1n} \cosh \Gamma_{1n}(z + d_1) \cos \frac{n\pi}{2b}(x + b) \quad \text{for } -d_1 < z < -d_2,$$

$$\begin{aligned}
 &= -\phi^i(x, z) + \sum_{n=0}^{\infty} \left[T_{mn}^- e^{\Gamma_{mn}(z+d_{m+1})} - T_{mn}^+ e^{-\Gamma_{mn}(z+d_{m+1})} \right] \\
 &\quad \cdot \cos \frac{n\pi}{2b}(x+b) \quad \text{for } -d_m < z < -d_{m+1} \quad (m = 2, 3, 4), \\
 &= -\phi^i(x, z) + \sum_{n=0}^{\infty} \left[T_n^- e^{\gamma_n(z+d_5)} - T_n^+ e^{-\gamma_n(z+d_5)} \right] \\
 &\quad \cdot \cos \frac{n\pi}{2b}(x+b) \quad \text{for } -d_5 < z < 0, \tag{49}
 \end{aligned}$$

where

$$\begin{aligned}
 T_{1n} &= \left(\frac{\pi}{2}\right)^{1/2} \frac{\nu_n e^{-\gamma_n d_5} e^{-\Gamma_{1n}(d_1-d_2)} P_{1n} U_{(+)}(i\gamma_n)}{b\Gamma_{1n}} \quad \text{for odd } n, \\
 &= -\left(\frac{\pi}{2}\right)^{1/2} \frac{\nu_n e^{-\gamma_n d_5} e^{-\Gamma_{1n}(d_1-d_2)} P_{1n} V_{(+)}(i\gamma_n)}{b\Gamma_{1n}} \quad \text{for even } n, \tag{50}
 \end{aligned}$$

$$\begin{aligned}
 T_{mn}^- &= -\left(\frac{\pi}{2}\right)^{1/2} \frac{\nu_n e^{-\gamma_n d_5} P_{mn} U_{(+)}(i\gamma_n)}{b\Gamma_{mn}} \quad \text{for odd } n \quad (m = 2, 3, 4), \\
 &= \left(\frac{\pi}{2}\right)^{1/2} \frac{\nu_n e^{-\gamma_n d_5} P_{mn} V_{(+)}(i\gamma_n)}{b\Gamma_{mn}} \quad \text{for even } n \quad (m = 2, 3, 4), \tag{51}
 \end{aligned}$$

$$\begin{aligned}
 T_{mn}^+ &= -\left(\frac{\pi}{2}\right)^{1/2} \frac{\nu_n e^{-\gamma_n d_5} Q_{mn} U_{(+)}(i\gamma_n)}{b\Gamma_{mn}} \quad \text{for odd } n \quad (m = 2, 3, 4), \\
 &= \left(\frac{\pi}{2}\right)^{1/2} \frac{\nu_n e^{-\gamma_n d_5} Q_{mn} V_{(+)}(i\gamma_n)}{b\Gamma_{mn}} \quad \text{for even } n \quad (m = 2, 3, 4), \tag{52}
 \end{aligned}$$

$$\begin{aligned}
 T_n^- &= -\left(\frac{\pi}{2}\right)^{1/2} \frac{\nu_n e^{-\gamma_n d_5} U_{(+)}(i\gamma_n)}{b\gamma_n} \quad \text{for odd } n, \\
 &= \left(\frac{\pi}{2}\right)^{1/2} \frac{\nu_n e^{-\gamma_n d_5} V_{(+)}(i\gamma_n)}{b\gamma_n} \quad \text{for even } n, \tag{53}
 \end{aligned}$$

$$T_n^+ = -\left(\frac{\pi}{2}\right)^{1/2} \frac{\nu_n e^{-\gamma_n d_5} Q_{4n} U_{(+)}(i\gamma_n)}{b\gamma_n} \quad \text{for odd } n,$$

$$= \left(\frac{\pi}{2}\right)^{1/2} \frac{\nu_n e^{-\gamma_n d_5} Q_{4n} V_{(+)}(i\gamma_n)}{b\gamma_n} \quad \text{for even } n, \quad (54)$$

In (50)–(54), P_{mn} and Q_{mn} for $m = 1, 2, 3$, and 4 are defined in Appendix A.

Next we shall consider the field outside the waveguide and derive a scattered far field for $|x| > b$. In view of (15), (28), (29), and (48), an integral representation of the scattered field for $x \gtrless \pm b$ is given by

$$\phi(x, z) = \mp (2\pi)^{-1/2} \int_{-\infty+ic}^{\infty+ic} \gamma^{-1} \Psi'_{(+)}(\pm b, \alpha) e^{-i\alpha z} d\alpha, \quad (55)$$

$$-k_2 < c < k_2 \cos \theta_0,$$

where

$$\Psi'_{(+)}(\pm b, \alpha) = \frac{U_{(+)}(\alpha) \pm V_{(+)}(\alpha)}{2}. \quad (56)$$

In order to evaluate (55), we express $\phi(x, z)$ as in

$$\phi(x, z) = \phi_1(x, z) + \phi_2(x, z), \quad (57)$$

where

$$\phi_1(x, z) = \pm (2\pi)^{-1/2} \int_{-\infty+ic}^{\infty+ic} \gamma^{-1} [\Psi'_{(+)}(\pm b, \alpha) - \tilde{\Phi}(\pm b, \alpha)] e^{\mp \gamma(x \mp b) - i\alpha z} d\alpha, \quad (58)$$

$$\phi_2(x, z) = \mp (2\pi)^{-1/2} \int_{-\infty+ic}^{\infty+ic} \gamma^{-1} \tilde{\Phi}(\pm b, \alpha) e^{\mp \gamma(x \mp b) - i\alpha z} d\alpha \quad (59)$$

for $x \gtrless \pm b$ with

$$\tilde{\Phi}(\pm b, \alpha) = \frac{k \sin \theta_0 e^{\mp ikb \sin \theta_0} (\alpha + k)^{1/2}}{(2\pi)^{1/2} (k + k \cos \theta_0)^{1/2} (\alpha - k \cos \theta_0)}. \quad (60)$$

For convenience, we now introduce the cylindrical coordinates $(\rho_{1,2}, \theta_{1,2})$ centered at the waveguide edges $(x, z) = (\pm b, 0)$ as follows:

$$x - b = \rho_1 \sin \theta_1, \quad z = \rho_1 \cos \theta_1 \quad \text{for } 0 < \theta_1 < \pi, \quad (61)$$

$$x + b = \rho_2 \sin \theta_2, \quad z = \rho_2 \cos \theta_2 \quad \text{for } -\pi < \theta_2 < 0. \quad (62)$$

In (57), $\phi_1(x, z)$ is evaluated asymptotically for large $|k|\rho_{1,2}$ with the aid of the saddle point method, whereas $\phi_2(x, z)$ is evaluated exactly

leading to the Fresnel integral representation. Omitting the details, we arrive at the asymptotic expression of (57) with the result that

$$\begin{aligned} & \phi(\rho_{1,2}, \theta_{1,2}) \\ & \sim \pm \left[\Psi'_{(+)}(\pm b, -k \cos \theta_{1,2}) - \tilde{\Phi}(\pm b, -k \cos \theta_{1,2}) \right] \frac{e^{i(k\rho_{1,2}-3\pi/4)}}{(k\rho_{1,2})^{1/2}} \\ & - e^{\mp ikb \sin \theta_0} \left\{ e^{-ik\rho_{1,2} \cos(\theta_{1,2}-\theta_0)} F \left[(2k\rho_{1,2})^{1/2} \cos \frac{\theta_{1,2}-\theta_0}{2} \right] \right. \\ & \left. - e^{-ik\rho_{1,2} \cos(\theta_{1,2}+\theta_0)} F \left[(2k\rho_{1,2})^{1/2} \cos \frac{\theta_{1,2}+\theta_0}{2} \right] \right\} \end{aligned} \quad (63)$$

as $k\rho_{1,2} \rightarrow \infty$ for $x \gtrless \pm b$, where $F(\cdot)$ is the Fresnel integral defined by

$$F(w) = \frac{e^{-i\pi/4}}{\pi^{1/2}} \int_w^\infty e^{it^2} dt. \quad (64)$$

Equation (63) gives a scattered far field expression uniformly valid in observation angles $\theta_{1,2}$.

An alternative asymptotic expression of (55) can be derived by using the cylindrical coordinate at the origin

$$x = \rho \sin \theta, \quad z = \rho \cos \theta \quad \text{for } -\pi < \theta < \pi \quad (65)$$

and applying the saddle point method. This yields,

$$\phi(\rho, \theta) \sim \phi_g(\rho, \theta) + \phi_d(\rho, \theta) \quad (66)$$

as $|k|\rho \rightarrow \infty$ for θ not too close to $\pm\pi \mp \theta_0$, where $\phi_g(\rho, \theta)$ and $\phi_d(\rho, \theta)$ are the geometrical optics field and the diffracted field, respectively, which are defined by

$$\begin{aligned} \phi_g(\rho, \theta) &= -e^{-ik\rho \cos(\theta-\theta_0)} \text{ for } -\pi < \theta_2 < -\pi + \theta_0, \\ &= 0 \text{ for } -\pi + \theta_0 < \theta_2 < 0, \quad 0 < \theta_1 < \pi - \theta_0, \\ &= e^{-2ikb \sin \theta_0} e^{-ik\rho \cos(\theta+\theta_0)} \text{ for } \pi - \theta_0 < \theta_1 < \pi, \end{aligned} \quad (67)$$

$$\phi_d(\rho, \theta) = \pm \Psi'_{(+)}(\pm b, -k \cos \theta) e^{\mp ikb \sin \theta} \frac{e^{i(k\rho-3\pi/4)}}{(k\rho)^{1/2}}, \quad \theta \gtrless 0. \quad (68)$$

Equation (66) is a non-uniform asymptotic expression of the scattered far field.

5. NUMERICAL RESULTS AND DISCUSSION

In this section, we shall present numerical examples of the RCS to discuss the far field backscattering characteristics of the waveguide

in detail. Since the cross section of the waveguide geometry under consideration is of infinite extent, the RCS per unit length is defined by

$$\sigma = \lim_{\rho \rightarrow \infty} \left(2\pi\rho \frac{|\phi^d|^2}{|\phi^i|^2} \right), \quad (69)$$

where ϕ^i and ϕ^d are the incident field and the diffracted field given by (2) and (68), respectively. For real k , (69) is simplified by using (28) and (29) as

$$\sigma = \frac{\lambda}{2} |U_{(+)}(-k \cos \theta) \pm V_{(+)}(-k \cos \theta)|^2 \quad (70)$$

for $\theta \geq 0$ with λ being the free-space wavelength.

Figures 2-5 show the normalized monostatic RCS σ/λ as a function of incidence angle θ_0 , where the values of σ/λ are plotted in decibels [dB] by computing $10 \log_{10} \sigma/\lambda$. In order to enable comparison between two different polarizations, we have chosen the same parameters as in the E -polarized case analyzed in [27]. The normalized waveguide aperture width kb and the waveguide dimension ratio $d_1/2b$ are taken as $kb = 3.14, 15.7, 31.4$ and $d_1/2b = 1.0, 3.0$, respectively. In numerical computation, we have chosen ferrite (single-layer material) [1] for region IV and Emerson & Cuming AN-73 (three-layer material) [1] for regions I-III to form the existing four-layer material loaded on the planar termination inside the waveguide (see Fig. 1). The material constants for ferrite and Emerson & Cuming AN-73 are $\varepsilon_4 = 2.4 + i1.25$, $\mu_4 = 1.6 + i0.9$ and $\varepsilon_1 = 3.14 + i10.0$, $\mu_1 = 1.0$, $\varepsilon_2 = 1.6 + i0.9$, $\mu_2 = 1.0$, $\varepsilon_3 = 1.4 + i0.35$, $\mu_3 = 1.0$, respectively, where the thickness of the three layers of Emerson & Cuming AN-73 and ferrite is such that $d_1 - d_2 = d_2 - d_3 = d_3 - d_4 = d_4 - d_5 (= \Delta)$. The normalized layer thickness is chosen as $k\Delta = 0.628, 1.255$. In order to investigate the effect of four-layer loading in detail, we have also computed the RCS for the single-layer case (region I: ferrite, regions II-IV: vacuum) and the three-layer case (regions I-III: Emerson & Cuming AN-73, region IV: vacuum). The results for no material loading (regions I-IV: vacuum) have also been added to enable comparison.

We shall first investigate the RCS reduction characteristics by comparing the results for empty and loaded cavities. It is seen from Figs. 2-5 that, as in the case of E polarization [27], the monostatic RCS exhibits fairly large values for cavities with no material loading due to the interior irradiation, whereas the RCS is reduced for the case of material loading inside the cavities. We also observe that this RCS reduction is noticeable for larger cavities. By comparing the RCS

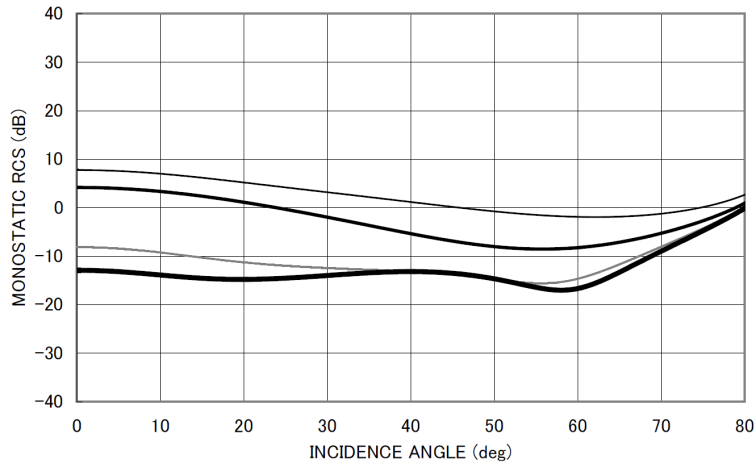


Figure 2(a). Monostatic RCS σ/λ [dB] for $d_1/2b = 1.0$, $kb = 3.14$, $k\Delta = 0.628$. —: cavity with no loading (regions I-IV: vacuum). —: cavity with single-layer loading (region I: ferrite, regions II-IV: vacuum). —: cavity with three-layer loading (regions I-III: Emerson & Cuming AN-73, region IV: vacuum). —: cavity with four-layer loading (regions I-III: Emerson & Cuming AN-73, region IV: ferrite).

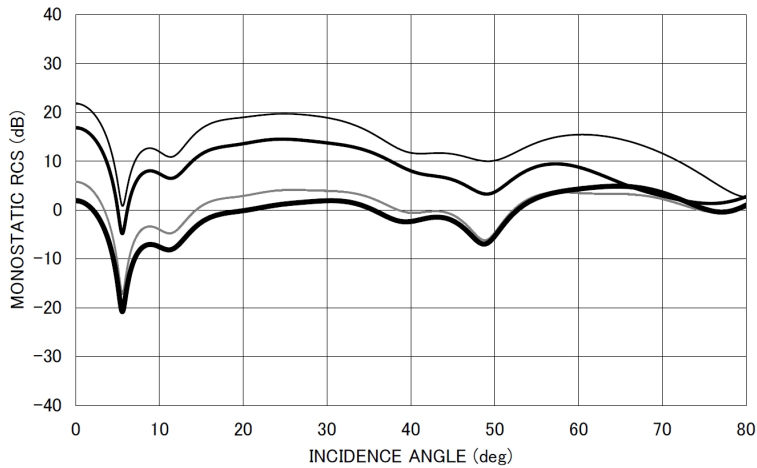


Figure 2(b). Monostatic RCS σ/λ [dB] for $d_1/2b = 1.0$, $kb = 15.7$, $k\Delta = 0.628$. Other particulars are the same as in Fig. 2(a).

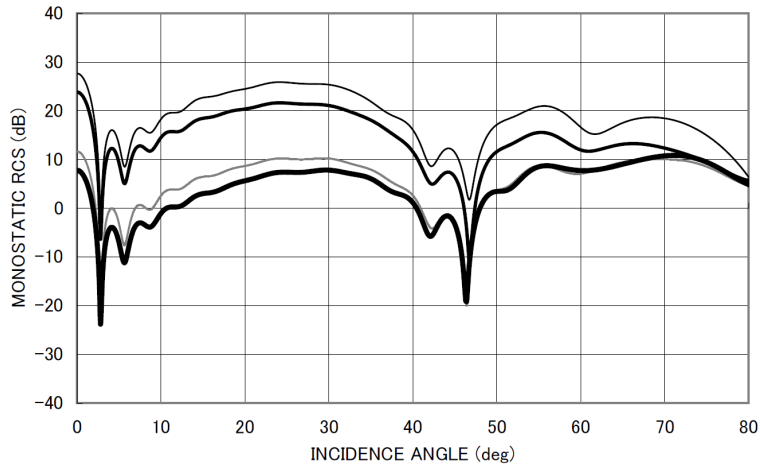


Figure 2(c). Monostatic RCS σ/λ [dB] for $d_1/2b = 1.0$, $kb = 31.4$, $k\Delta = 0.628$. Other particulars are the same as in Fig. 2(a).

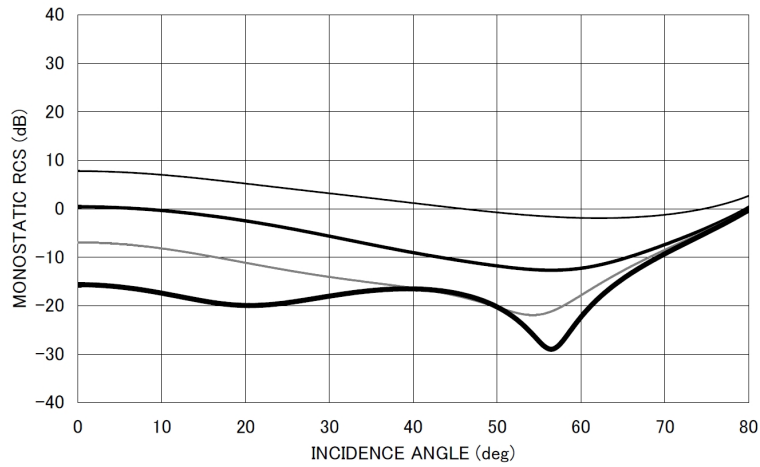


Figure 3(a). Monostatic RCS σ/λ [dB] for $d_1/2b = 3.0$, $kb = 3.14$, $k\Delta = 0.628$. Other particulars are the same as in Fig. 2(a).

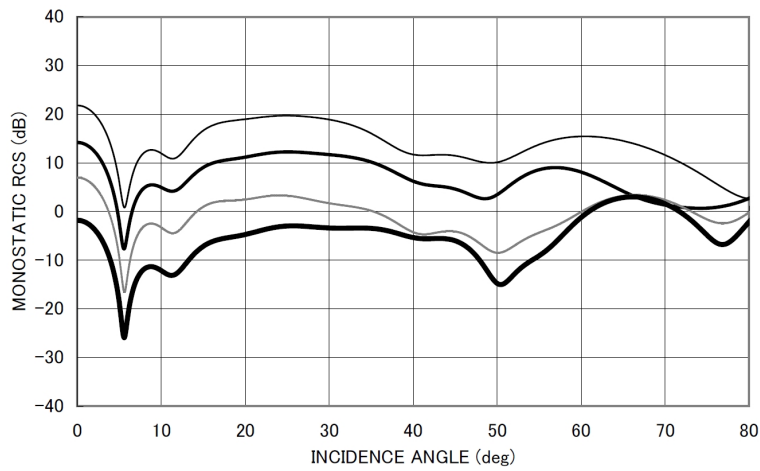


Figure 3(b). Monostatic RCS σ/λ [dB] for $d_1/2b = 3.0$, $kb = 15.7$, $k\Delta = 0.628$. Other particulars are the same as in Fig. 2(a).

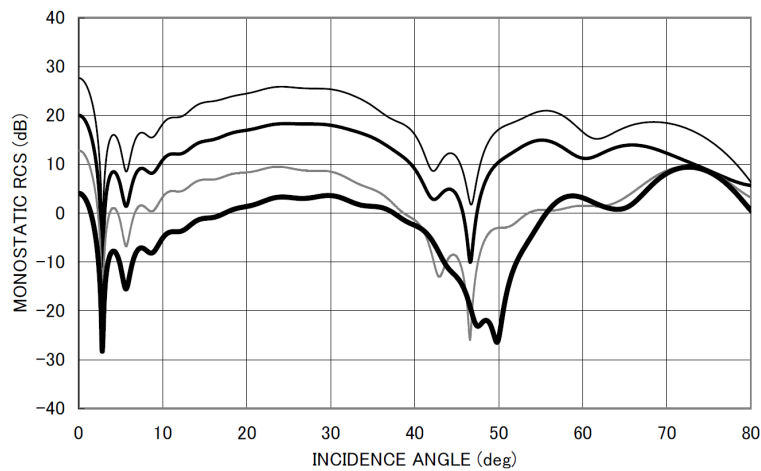


Figure 3(c). Monostatic RCS σ/λ [dB] for $d_1/2b = 3.0$, $kb = 31.4$, $k\Delta = 0.628$. Other particulars are the same as in Fig. 2(a).

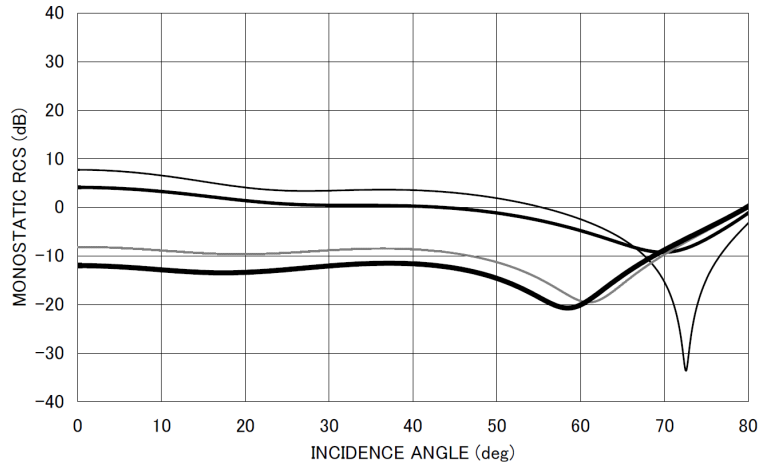


Figure 4(a). Monostatic RCS σ/λ [dB] for $d_1/2b = 1.0$, $kb = 3.14$, $k\Delta = 1.255$. —: cavity with no loading (regions I-IV: vacuum). —: cavity with single-layer loading (region I: ferrite, regions II-IV: vacuum). - - -: cavity with three-layer loading (regions I-III: Emerson & Cuming AN-73, region IV: vacuum). —: cavity with four-layer loading (regions I-III: Emerson & Cuming AN-73, region IV: ferrite).

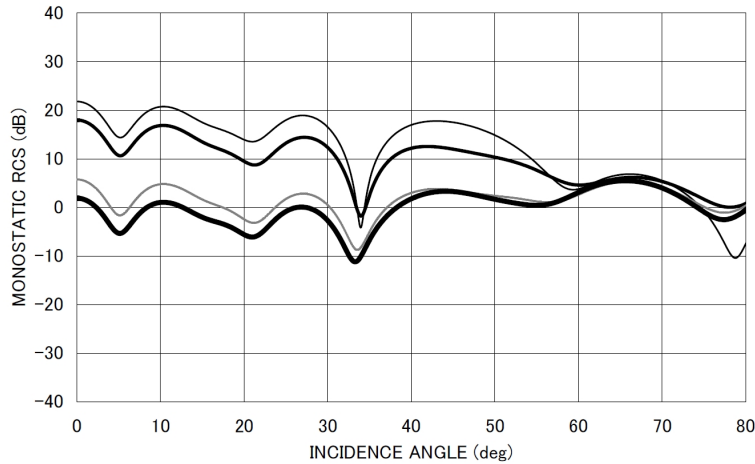


Figure 4(b). Monostatic RCS σ/λ [dB] for $d_1/2b = 1.0$, $kb = 15.7$, $k\Delta = 1.255$. Other particulars are the same as in Fig. 4(a).

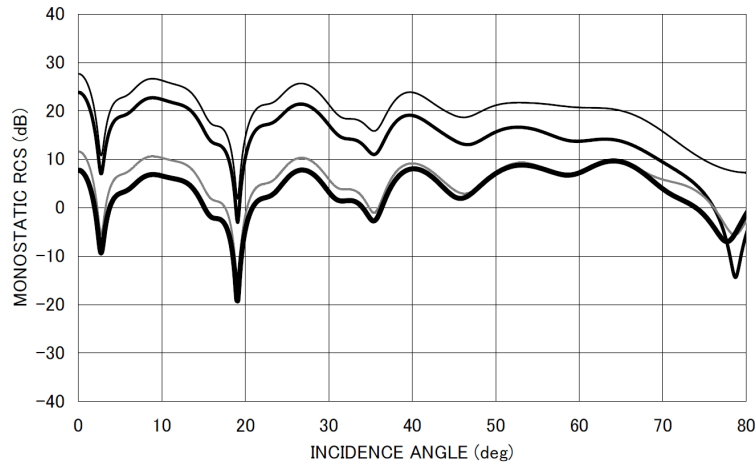


Figure 4(c). Monostatic RCS σ/λ [dB] for $d_1/2b = 1.0$, $kb = 31.4$, $k\Delta = 1.255$. Other particulars are the same as in Fig. 4(a).

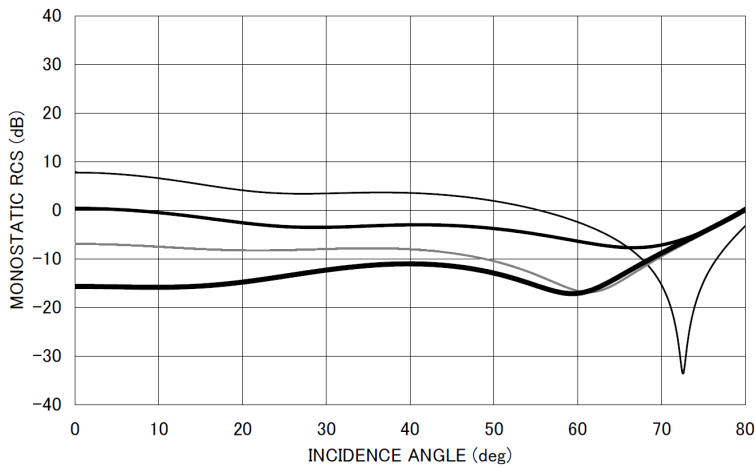


Figure 5(a). Monostatic RCS σ/λ [dB] for $d_1/2b = 3.0$, $kb = 3.14$, $k\Delta = 1.255$. Other particulars are the same as in Fig. 4(a).

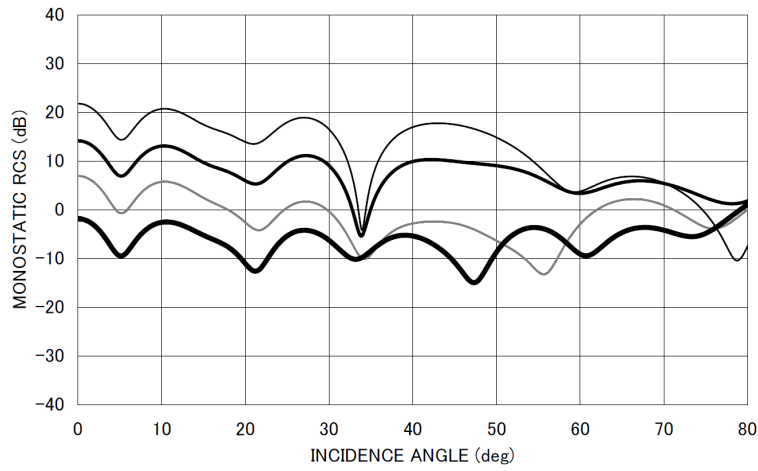


Figure 5(b). Monostatic RCS σ/λ [dB] for $d_1/2b = 3.0$, $kb = 15.7$, $k\Delta = 1.255$. Other particulars are the same as in Fig. 4(a).

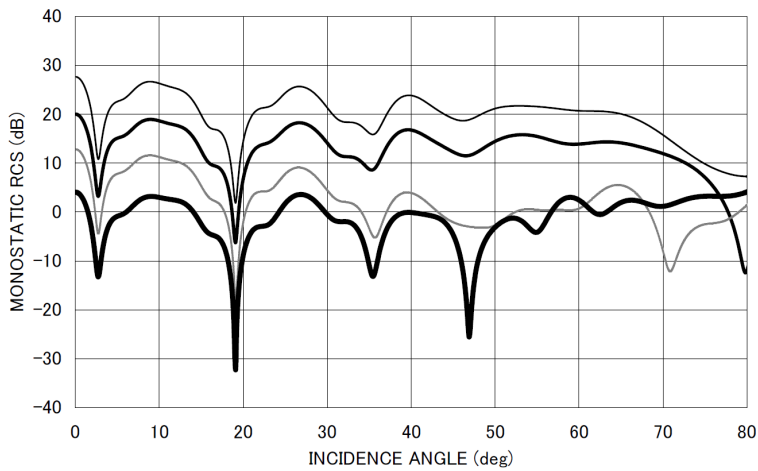


Figure 5(c). Monostatic RCS σ/λ [dB] for $d_1/2b = 3.0$, $kb = 31.4$, $k\Delta = 1.255$. Other particulars are the same as in Fig. 4(a).

results for material-loaded cavities between the single- and four-layer cases, it is found that the RCS reduction is more significant in the four-layer case. Similarly by comparing the results for the four-layer case with those for the three-layer case, more RCS reduction is seen in the four-layer case. From these characteristics, it is expected that the multi-layer loading gives rise to better RCS reduction over a broad frequency range.

Let us now make comparisons of the monostatic RCS results between two different polarizations. As mentioned earlier, we have analyzed the E -polarized plane wave diffraction by the same waveguide in our previous paper [27]. Comparing the RCS curves in Figs. 2–5 for the H polarization with those in Figs. 2–5 in [27] for the E polarization, we see differences in all numerical examples. In particular, the monostatic RCS for the H polarization oscillates rapidly in comparison to the E -polarized case. This difference is due to the fact that the effect of edge diffraction depends on the incident polarization. We also see that, if the waveguide aperture opening is small as in $kb = 3.14$, there are great differences in the RCS characteristics between the H polarization (Figs. 2–5 in this paper) and the E polarization (Figs. 2–5 in [27]). This is because the diffraction phenomena at low frequencies strongly depend on the incident polarization. It is also found that, with an increase of the waveguide aperture opening, the RCS for E and H polarizations exhibits close features to each other. Comparing the results between $k\Delta = 0.628$ and 1.255 , the RCS reduction is noticeable with an increase of the material thickness for both polarizations.

6. CONCLUSIONS

In this paper, we have rigorously analyzed the H -polarized plane wave diffraction by a terminated, semi-infinite parallel-plate waveguide with four-layer material loading using the Wiener-Hopf technique. Exact and approximate solutions of the Wiener-Hopf equations have been obtained. Explicit expressions of the scattered field inside and outside the waveguide have been derived analytically. In particular, the field outside the waveguide has been evaluated with the aid of the saddle point method leading to the far field asymptotic expressions in two different forms. It is to be noted that our final solution obtained in this paper is valid for arbitrary cavity dimensions. We have presented illustrative numerical examples on the monostatic RCS to discuss the far field backscattering characteristics of the waveguide in detail. In particular, it has been clarified that, as in the E -polarized case [27], the four-layer loading inside the cavity results in better RCS reduction compared with the three-layer case. Some comparisons between two

different polarizations have also been made.

APPENDIX A. ON THE COEFFICIENTS f_n^+ , f_{mn} , AND g_{mn} FOR $n = 1, 2, 3, \dots$ WITH $m = 1, 2, 3, 4$ IN (22)–(25)

The coefficients f_n^+ , f_{mn} and g_{mn} for $n = 1, 2, 3, \dots$ with $m = 1, 2, 3, 4$ have appeared in the scattered field expression (15) (see (22)–(25)). These are given as

$$\begin{aligned} f_n^+ &= \frac{n\pi}{2b} e^{-\Gamma_{1n}(d_1-d_2)} e^{-\gamma_n d_5} P_{1n} U_{(+)}(i\gamma_n) \quad \text{for odd } n, \\ &= -\frac{n\pi}{2b} e^{-\Gamma_{1n}(d_1-d_2)} e^{-\gamma_n d_5} P_{1n} V_{(+)}(i\gamma_n) \quad \text{for even } n, \end{aligned} \quad (\text{A1})$$

$$\begin{aligned} f_{mn} &= \frac{n\pi}{2b} P_{mn} U_{(+)}(i\gamma_n) \quad \text{for odd } n, \\ &= -\frac{n\pi}{2b} P_{mn} V_{(+)}(i\gamma_n) \quad \text{for even } n, \end{aligned} \quad (\text{A2})$$

$$\begin{aligned} g_{mn} &= \frac{n\pi}{2b} Q_{mn} U_{(+)}(i\gamma_n) \quad \text{for odd } n, \\ &= -\frac{n\pi}{2b} Q_{mn} V_{(+)}(i\gamma_n) \quad \text{for even } n, \end{aligned} \quad (\text{A3})$$

where P_{mn} and Q_{mn} are defined by

$$P_{4n} = \frac{(1 + \rho_{4n}) [1 - e^{-2\Gamma_{4n}(d_4-d_5)} \rho_{3n}]}{\rho_{4n} [1 - e^{2\Gamma_{4n}(d_4-d_5)} \rho_{3n} \rho_{4n}]} \frac{\Gamma_{4n} \varepsilon_4}{\gamma_n \varepsilon_4 + \Gamma_{4n}}, \quad (\text{A4})$$

$$Q_{4n} = \frac{e^{-2\Gamma_{4n}(d_4-d_5)} \rho_{3n} - \rho_{4n}}{1 - e^{-2\Gamma_{4n}(d_4-d_5)} \rho_{3n} \rho_{4n}}, \quad (\text{A5})$$

$$P_{3n} = \frac{(1 - \rho_{4n}) e^{-\Gamma_{4n}(d_4-d_5)}}{1 - e^{-2\Gamma_{4n}(d_4-d_5)} \rho_{3n} \rho_{4n}} \frac{(1 + \delta_{2n}) \Gamma_{3n} \varepsilon_4}{(\varepsilon_4/\varepsilon_3) \Gamma_{3n} + \delta_{2n} \Gamma_{4n}}, \quad (\text{A6})$$

$$Q_{3n} = \frac{e^{-\Gamma_{4n}(d_4-d_5)} \rho_{3n} (1 - \rho_{4n}) \varepsilon_4 \Gamma_{3n}}{1 - e^{-2\Gamma_{4n}(d_4-d_5)} \rho_{3n} \rho_{4n}}, \quad (\text{A7})$$

$$\begin{aligned} P_{2n} &= \frac{(1 + \delta_{1n}) \Gamma_{2n} e^{-\Gamma_{3n}(d_3-d_4)}}{(\varepsilon_3/\varepsilon_2) \Gamma_{2n} + \delta_{1n} \Gamma_{3n}} \\ &\quad \cdot \frac{(1 - \rho_{4n}) e^{-\Gamma_{4n}(d_4-d_5)}}{1 - e^{-2\Gamma_{4n}(d_4-d_5)} \rho_{3n} \rho_{4n}} \frac{(1 + \delta_{2n}) \Gamma_{3n} \varepsilon_4}{(\varepsilon_4/\varepsilon_3) \Gamma_{3n} + \delta_{2n} \Gamma_{4n}}, \end{aligned} \quad (\text{A8})$$

$$Q_{2n} = \frac{e^{-\Gamma_{3n}(d_3-d_4)} \rho_{2n} e^{-\Gamma_{4n}(d_4-d_5)} (1 - \rho_{4n})}{1 - e^{-2\Gamma_{4n}(d_4-d_5)} \rho_{3n} \rho_{4n}} \frac{\varepsilon_4 \Gamma_{3n}}{(\varepsilon_4/\varepsilon_3) \Gamma_{3n} + \delta_{2n} \Gamma_{4n}}, \quad (\text{A9})$$

$$P_{1n} = \frac{(K_n + \Gamma_{1n}) e^{-\Gamma_{2n}(d_2-d_3)} (1 + \delta_{1n}) \Gamma_{2n} e^{-\Gamma_{3n}(d_3-d_4)}}{(\varepsilon_2/\varepsilon_1) K_n + \Gamma_{2n} (\varepsilon_3/\varepsilon_2) \Gamma_{2n} + \delta_{1n} \Gamma_{3n}} \cdot \frac{(1 - \rho_{4n}) e^{-\Gamma_{4n}(d_4-d_5)} (1 + \delta_{2n}) \Gamma_{3n} \varepsilon_4}{1 - e^{-2\Gamma_{4n}(d_4-d_5)} \rho_{3n} \rho_{4n} (\varepsilon_4/\varepsilon_3) \Gamma_{3n} + \delta_{2n} \Gamma_{4n}}, \quad (\text{A10})$$

$$Q_{1n} = \frac{e^{-\Gamma_{2n}(d_2-d_3)} \rho_{1n} (1 + \delta_{1n}) \Gamma_{2n}}{(\varepsilon_2/\varepsilon_1) \Gamma_{2n} + \delta_{1n} \Gamma_{3n}} \cdot \frac{e^{-\Gamma_{3n}(d_3-d_4)} e^{-\Gamma_{4n}(d_4-d_5)} (1 - \delta_{3n}) \varepsilon_4 \Gamma_{3n}}{1 - e^{-2\Gamma_{4n}(d_4-d_5)} \rho_{3n} \rho_{4n} (\varepsilon_4/\varepsilon_3) \Gamma_{3n} + \delta_{2n} \Gamma_{4n}}, \quad (\text{A11})$$

where

$$K_n = \frac{\Gamma_{1n} + e^{-2\Gamma_{1n}(d_1-d_2)}}{1 - e^{-2\Gamma_{1n}(d_1-d_2)}}, \quad (\text{A12})$$

$$\rho_{1n} = \frac{(\varepsilon_2/\varepsilon_1) K_n - \Gamma_{2n}}{(\varepsilon_2/\varepsilon_1) K_n + \Gamma_{2n}}, \quad (\text{A13})$$

$$\delta_{1n} = \frac{1 - \rho_{1n} e^{-2\Gamma_{2n}(d_2-d_3)}}{1 + \rho_{1n} e^{-2\Gamma_{2n}(d_2-d_3)}}, \quad (\text{A14})$$

$$\rho_{2n} = \frac{(\varepsilon_3/\varepsilon_2) \Gamma_{2n} - \delta_{1n} \Gamma_{3n}}{(\varepsilon_3/\varepsilon_2) \Gamma_{2n} + \delta_{1n} \Gamma_{3n}}, \quad (\text{A15})$$

$$\delta_{2n} = \frac{1 - \rho_{2n} e^{-2\Gamma_{3n}(d_3-d_4)}}{1 + \rho_{2n} e^{-2\Gamma_{3n}(d_3-d_4)}}, \quad (\text{A16})$$

$$\rho_{3n} = \frac{(\varepsilon_4/\varepsilon_3) \Gamma_{3n} - \delta_{2n} \Gamma_{4n}}{(\varepsilon_4/\varepsilon_3) \Gamma_{3n} + \delta_{2n} \Gamma_{4n}}, \quad (\text{A17})$$

$$\rho_{4n} = \frac{\varepsilon_4 \gamma_n - \Gamma_{4n}}{\varepsilon_4 \gamma_n + \Gamma_{4n}}. \quad (\text{A18})$$

Substituting (A2) and (A3) with $m = 4$ into (21) and setting $\alpha = -i\gamma_n$, we also find that

$$\begin{aligned} c_{5n}(-i\gamma_n) &= \frac{n\pi}{2b} \delta_n U_{(+)}(i\gamma_n) \quad \text{for odd } n, \\ &= -\frac{n\pi}{2b} \delta_n V_{(+)}(i\gamma_n) \quad \text{for even } n, \end{aligned} \quad (\text{A19})$$

where

$$\delta_n = \frac{[\rho_{3n} e^{-2\Gamma_{4n}(d_4-d_5)} - \rho_{4n}] e^{-2\gamma_n d_5}}{1 - \rho_{3n} \rho_{4n} e^{-2\Gamma_{4n}(d_4-d_5)}}. \quad (\text{A20})$$

REFERENCES

1. Lee, S.-W. and H. Ling, "Data book for cavity RCS: Version 1," Tech. Rep., No. SWL 89-1, Univ. Illinois, Urbana, 1989.
2. Lee, S.-W. and R. J. Marhefka, "Data book of high-frequency RCS: Version 2," Tech. Rep., Univ. Illinois, Urbana, 1989.
3. Stone, W. R., Ed., *Radar Cross Sections of Complex Objects*, IEEE Press, New York, 1990.
4. Bernard, J. M. L., G. Pelosi, and P. Ya. Ufimtsev, Eds., *Special Issue on Radar Cross Section of Complex Objects, Ann. Telecommun.*, Vol. 50, No. 5-6, 1995.
5. Lee, C. S. and S.-W. Lee, "RCS of a coated circular waveguide terminated by a perfect conductor," *IEEE Trans. Antennas Propagat.*, Vol. 35, No. 4, 391-398, 1987.
6. Altıntaş A., P. H. Pathak, and M. C. Liang, "A selective modal scheme for the analysis of EM coupling into or radiation from large open-ended waveguides," *IEEE Trans. Antennas Propagat.*, Vol. 36, No. 1, 84-96, 1988.
7. Ling, H., R.-C. Chou, and S.-W. Lee, "Shooting and bouncing rays: Calculating the RCS of an arbitrary shaped cavity," *IEEE Trans. Antennas Propagat.*, Vol. 37, No. 2, 194-205, 1989.
8. Pathak, P. H. and R. J. Burkholder, "Modal, ray, and beam techniques for analyzing the EM scattering by open-ended waveguide cavities," *IEEE Trans. Antennas Propagat.*, Vol. 37, No. 5, 635-647, 1989.
9. Pathak, P. H. and R. J. Burkholder, "A reciprocity formulation for the EM scattering by an obstacle within a large open cavity," *IEEE Trans. Microwave Theory Tech.*, Vol. 41, No. 4, 702-707, 1993.
10. Lee, R. and T.-T. Chia, "Analysis of electromagnetic scattering from a cavity with a complex termination by means of a hybrid ray-FDTD method," *IEEE Trans. Antennas Propagat.*, Vol. 41, No. 11, 1560-1569, 1993.
11. Ohnuki, S. and T. Hinata, "Radar cross section of an open-ended rectangular cylinder with an iris inside the cavity," *IEICE Trans. Electron.*, Vol. E81-C, No. 12, 1875-1880, 1998.
12. Noble, B., *Methods Based on the Wiener-Hopf Technique for the Solution of Partial Differential Equations*, Pergamon, London, 1958.
13. Mittra, R. and S.-W. Lee, *Analytical Techniques in the Theory of Guided Waves*, Macmillan, New York, 1971.

14. Kobayashi, K., "Wiener-Hopf and modified residue calculus techniques," *Analysis Methods for Electromagnetic Wave Problems*, Chap. 8, Yamashita, E., Ed., Artech House, Boston, 1990.
15. Büyükaksoy, A., F. Birbir, and E. Erdoğan, "Scattering characteristics of a rectangular groove in a reactive surface," *IEEE Trans. Antennas and Propagat.*, Vol. 43, No. 12, 1450–1458, 1995.
16. Çetiner, B. A., A. Büyükaksoy, and F. Güneş, "Diffraction of electromagnetic waves by an open ended parallel plate waveguide cavity with impedance walls," *Progress In Electromagnetics Research*, PIER 26, 165–197, 2000.
17. Kobayashi, K. and A. Sawai, "Plane wave diffraction by an open-ended parallel plate waveguide cavity," *Journal of Electromagnetic Waves and Applications*, Vol. 6, No. 4, 475–512, 1992.
18. Kobayashi, K., S. Koshikawa, and A. Sawai, "Diffraction by a parallel-plate waveguide cavity with dielectric/ferrite loading: Part I — The case of E polarization," *Progress In Electromagnetics Research*, PIER 8, 377–426, 1994.
19. Koshikawa, S. and K. Kobayashi, "Diffraction by a parallel-plate waveguide cavity with dielectric/ferrite loading: Part II — The case of H polarization," *Progress In Electromagnetics Research*, PIER 8, 427–458, 1994.
20. Koshikawa, S., T. Momose, and K. Kobayashi, "RCS of a parallel-plate waveguide cavity with three-layer material loading," *IEICE Trans. Electron.*, Vol. E77-C, No. 9, 1514–1521, 1994.
21. Okada, S., S. Koshikawa, and K. Kobayashi, "Wiener-Hopf analysis of the plane wave diffraction by a finite parallel-plate waveguide with three-layer material loading: Part I — The case of E polarization," *Telecommunications and Radio Engineering*, Vol. 58, No. 1&2, 53–65, 2002.
22. Okada, S., S. Koshikawa, and K. Kobayashi, "Wiener-Hopf analysis of the plane wave diffraction by a finite parallel-plate waveguide with three-layer material loading: Part II — The case of H polarization," *Telecommunications and Radio Engineering*, Vol. 58, No. 1&2, 66–75, 2002.
23. Zheng, J. P. and K. Kobayashi, "Plane wave diffraction by a finite parallel-plate waveguide with four-layer material loading: Part I — The case of E polarization," *Progress In Electromagnetics Research B*, Vol. 6, 1–36, 2008.
24. Shang, E. H. and K. Kobayashi, "Plane wave diffraction by a finite parallel-plate waveguide with four-layer material loading: Part II — The case of H polarization," *Progress In Electromagnetics Research B*, Vol. 6, 267–294, 2008.

25. Koshikawa, S. and K. Kobayashi, "Diffraction by a terminated, semi-infinite parallel-plate waveguide with three-layer material loading," *IEEE Trans. Antennas and Propagat.*, Vol. 45, No. 6, 949–959, 1997.
26. Koshikawa, S. and K. Kobayashi, "Diffraction by a terminated, semi-infinite parallel-plate waveguide with three-layer material loading; the case of H polarization," *Electromagnetic Waves & Electronic Systems*, Vol. 5, No. 1, 13–23, 2000.
27. Shang, E. H. and K. Kobayashi, "Diffraction by a terminated, semi-infinite parallel-plate waveguide with four-layer material loading," *Progress In Electromagnetics Research B*, accepted for publication.